Journal of Radioanalytical and Nuclear Chemistry (2020) 325:365–379
https://doi.org/10.1007/s10967-020-07247-w

Hydrogeochemical characteristics of a closed karst groundwater basin in North China

Yongli Guo[1,2] · Cheng Zhang[1,2] · Qiong Xiao[1,2] · Hua Bu[3]

Received: 18 January 2020 / Published online: 8 June 2020

Abstract
Understanding the hydrogeochemical processes of carbonate aquifers is essential for utilizing local karst groundwater resources sustainability. Integrating hydrochemistry, environmental isotopes and hydrogeological conditions was used to study hydrogeochemical characteristics of a closed karst groundwater basin located in Shandong Province, North China. The dominant hydrochemistry type was HCO_3–SO_4–Ca in the karst groundwater system. Carbonates dissolution (especially calcite dissolution) as the main rock chemical weathering dominated the chemical compositions of the carbonate aquifers. Hydrogeochemical evolution processes of the closed karst groundwater basin were mainly carbonates dissolution accompanied with weak influences of human activities and weak evaporation during the recharging of atmospheric precipitation.

Keywords Hydrogeochemical characteristics · A closed karst groundwater basin · Carbonates dissolution · Human activities · Weak evaporation

Introduction

Groundwater resource plays a vital role in the agricultural, industrial and domestic activities of humans, it accounts for ~ 98% of the Earth's available fresh water [1]. Among them, karst groundwater is used as a drinking water source for approximately 25% of the world's population [2, 3]. Karst aquifers are characterized by highly heterogeneous functioning and are different from fractured and granular aquifers, thereby it is difficult to obtain hydrogeological parameters of karst aquifers and hard to build accurately numerical simulations of water flow and solute transportation in karst areas [4]. It is worthy to notice that water chemistries and isotopes as natural tracers of karst groundwater system could provide supplementary information to trace hydrogeological conditions in karst areas [5], they are equally useful to understand characteristics of karstified aquifers compared with groundwater numerical simulation models [6]. Hydrogeochemical analyses of karst groundwater system has been successfully used to reveal groundwater flow paths, groundwater circulation depth, groundwater resources composition, groundwater vulnerability, water-rock interactions, hydrogeochemical evolution and other hydrodynamic processes [7–14].

Karst aquifers in North China belongs to arid and semi-arid climatic zones, they are mainly buried and are of Cambrian-Ordovician carbonate formations. These karst groundwater systems have stable groundwater flow, relatively good groundwater quality and large volume storage of groundwater, they are the most important urban water supplies in local areas [3, 15]. Thus, understanding the hydrogeological evolution characteristics of a typical karst groundwater system in North China is extremely valuable for the sustainable utilization of karst groundwater resources. Yangzhuang karst groundwater basin is a typical closed groundwater system in Shandong Province, North China, its hydrogeochemical characteristics could represent the carbonate aquifer system of karst critical zone in North China. Several hydrogeological studies have published. Bu et al. [16] chose the NO_3^- as the indicator to divide the karst groundwater source protection areas. Fu et al. [17] used the simulation method to

✉ Yongli Guo
gylguo@karst.ac.cn

✉ Cheng Zhang
chzhang@karst.ac.cn

1 Institute of Karst Geology, Chinese Academy of Geological Sciences/Key Laboratory of Karst Dynamics, MNR and GZAR, Guilin 541004, People's Republic of China

2 International Research Center on Karst under the Auspices of UNESCO, Guilin 541004, People's Republic of China

3 Shandong Lunan Geological Engineering Investigation Institute, Yanzhou 272100, People's Republic of China

determine the exploitation potential and the optimal exploitation of groundwater resources. Feng and Li [18] used several parameters [TH (Total hardness), TDS (Total dissolved solids), Cl^-, SO_4^{2-}] in 1980 and 2016 to study the variations of groundwater environment. The paper was focused on the hydrogeochemical processes of Yangzhuang karst groundwater basin, in order to guide local managers to utilize karst groundwater and optimize the spatial land use reasonably.

Integrating hydrochemistry, environmental isotopes and hydrogeological conditions was used in the paper to provide insights into the hydrogeological characteristics of Yangzhuang karst groundwater basin in North China Plain. Research goals of the paper were to identify the subsurface hydrogeochemical evolution processes of the typical closed karst groundwater system. The results are essential for ensuring the drinking-water supply security, they are also especially important to support sustainable management of the water resources and satisfy the demands of future generations.

Study area

Hydrogeological characteristics

The closed groundwater reservoir is defined as a natural confined aquifer system with an ideal water-storing space and its own complete recharge, run-off and discharge conditions, it not only has large volume of storage and regulation in groundwater, but also has natural functions of supplying and transporting groundwater resources. Karst areas are not well developed and heterogeneously distributed in North China. Yangzhuang karst groundwater basin with a narrow exit is a typical closed groundwater reservoir with excellent conductivity and regulation effect, it is one of the representative karst aquifer systems of North China [17], its hydrodynamic field is basically uniform. Several groundwater resources fields have been established and are being explored extensively, which have great contributions to the regional economy and living standards.

Yangzhuang karst groundwater system is a synclinal basin amidst mountains in Shandong Province with an area of ~ 650 km^2 (Fig. 1) [17], it has the complete recharge, run-off and discharge conditions. Hydrogeological cross-section map of A−A′ in Fig. 1a from southwest to northeast was shown in Fig. 1b. The strata are dominated by carbonates and are inclined towards the center of the basin. Surface watersheds of Cambrian limestones, metamorphic rocks and magmatic rocks exist in the northwest, north and east of the basin (Fig. 1). There exists a 15.4 km-long, 375–1500 m-wide Quaternary paleochannel in the central part of the basin. The spatial distribution of aquifers yield property in different aquifers was shown in Fig. 1a, it could reflect karst development characteristics of carbonate aquifers in the basin [19], the higher the yield property is, the more the karst development is. The yield property of aquifers becomes larger and larger from northeast to southwest, and the Ordovician aquifers have relatively larger yield property than others.

Precipitation is the mainly recharge source of groundwater and surface water in the basin. Generally, groundwater flows from northeast towards southwest. Groundwater resources are mainly discharged in ways of springs and artificial exploration. As the only seasonal surface river, Xinxue River cuts deep into the ground, lots of its segments are discharged and recharged together with groundwater, and the river becomes the major channel for groundwater recharge and discharge [17]. Water level of Xinxue River changes with time in the year. The Xinxue Rive with higher level recharges groundwater, while groundwater with higher level recharges Xinxue River. The recharging relationship between Xinxue Rive and groundwater changes with time and space.

Yangzhuang karst groundwater basin is divided into three small hydrogeological units (including Xinzhao, Shanting and Yangzhuang blocks) by faults (Fig. 1a). Each unit has its own hydrogeological conditions. Xinzhao and Shanting blocks located in the upper and middle reaches are recharge-runoff areas with the lack of groundwater quantity, where have higher altitude and larger landform undulates. Yangzhuang block lies in the lower reaches of Xinxue River and downstream of the basin, it stores most quantity of karst groundwater resources in the basin, and its groundwater circulation and aquifer yield property outperform other blocks.

Dynamic variation of hydrological conditions

Yangzhuang karst groundwater basin belongs to the warm continental monsoon climate zone with distinct four seasons, the annual average temperature is 14 °C. The annual average rainfall and evaporation are 768 mm and 1820 mm, respectively. The rainy season occurs from June to September, total precipitation in the period accounts for 70–80% of the annual total.

There are three groundwater level monitoring points in the basin from upstream to downstream (a → b → c) (Fig. 1), variation processes between precipitation and groundwater levels of three monitoring points changing with time were plotted in Fig. 2.

Dynamics of groundwater levels in the recharge areas dominated by the annual precipitation is in a natural balance state basically (Fig. 2a). Carbonates have stronger karst development in the runoff areas where have higher hydraulic conductivity and water abundance. Even though dynamics of

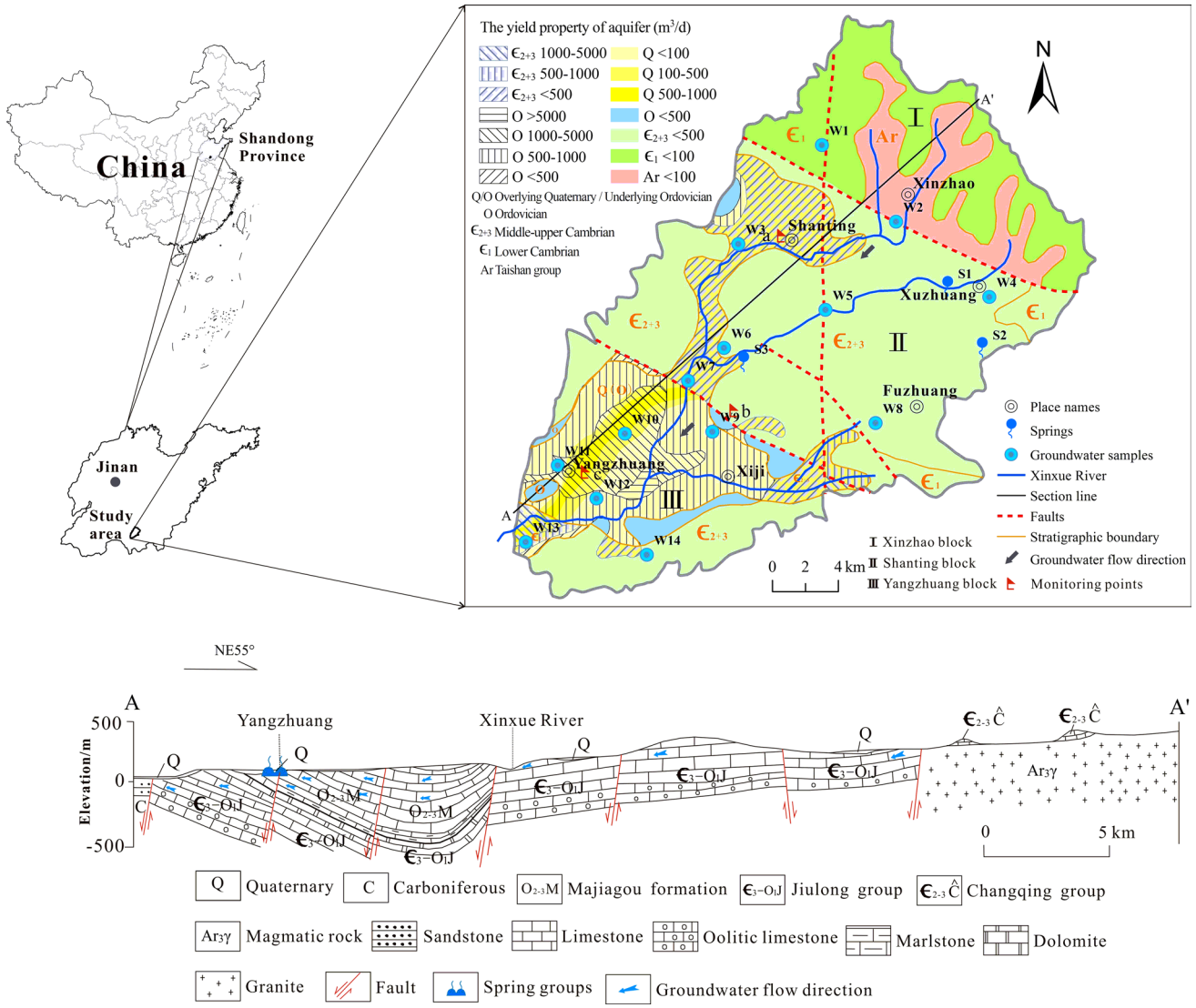

Fig. 1 The study area **a** hydrohgeological map of Yangzhuang karst groundwater basin and sampling points; **b** Hydrogeological cross-section of A−A′ in the basin

groundwater levels in the runoff areas is influenced by precipitation and artificial exploitation for the cultivated land covering the area mostly, it is still in a dynamic balance state (Fig. 2b). The discharge areas with the most quantity of karst groundwater are the main groundwater supply sources for the local inhabitants, which have the strongest karst development and the best connectivity. Groundwater has many recharge sources and the strongest self-adjustment ability in discharge areas, and groundwater levels are also in a dynamic balance state with characteristics of stable and seasonal ascending and descending (Fig. 2c).

Materials and methods

Sampling and analyses

The research work tried to select all groundwater bodies stored in different carbonate geological formations from upstream to downstream to obtain the hydrogeological characteristics of the basin comprehensively. Seventeen water samples including fourteen groundwater wells and three springs samples were collected in March, 2019 (Fig. 1a). Their information was summarized in Table 1.

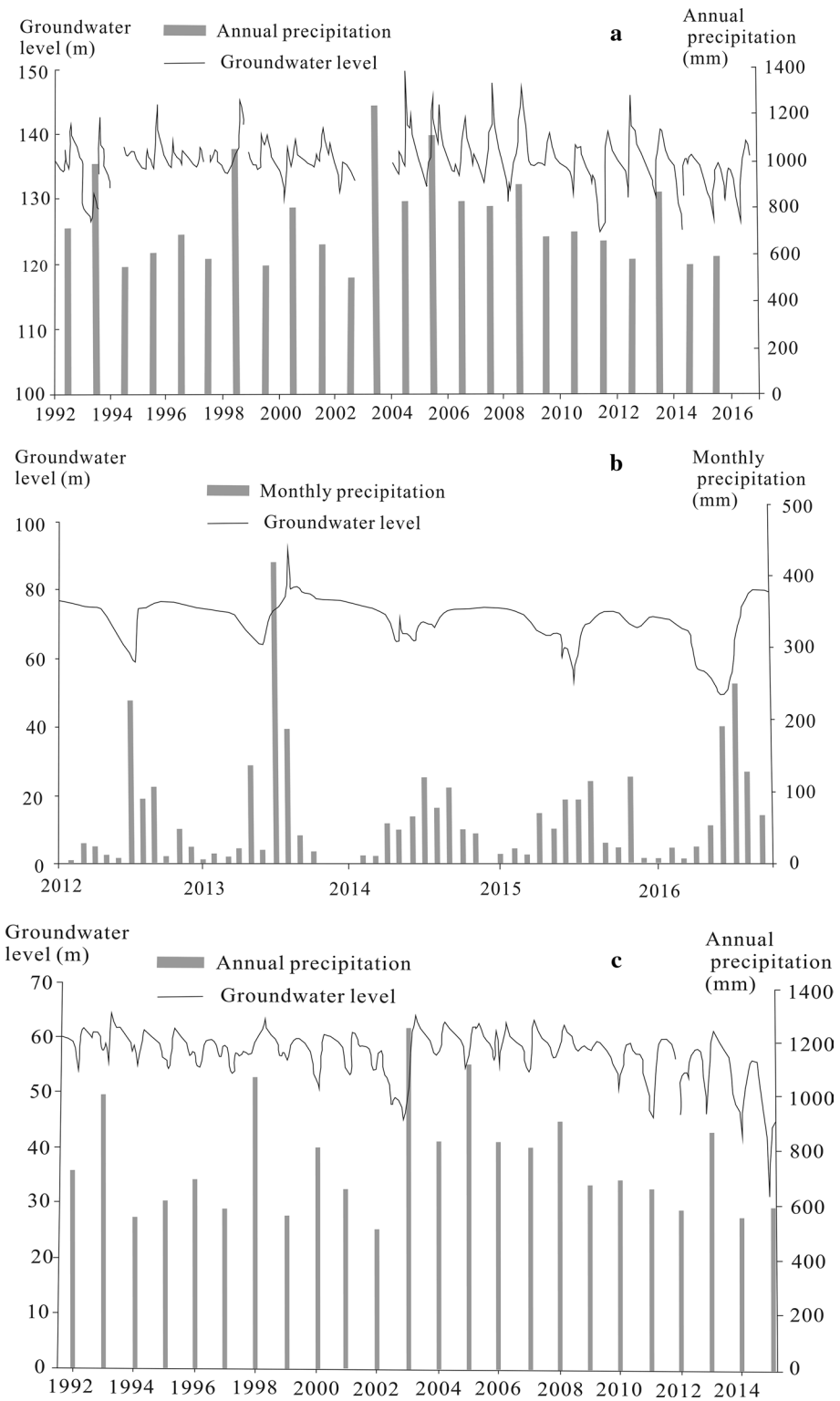

Fig. 2 Groundwater levels vary with precipitation over time from upstream to downstream (**a** the recharge areas, **b** the run-off areas, **c** the discharge areas)

Values of T (°C), pH, electrical conductivity (EC, μs cm^{-1}) and total dissolved solids (TDS, mg L^{-1}) of water samples were measured in the field using a multiparameter probe (PONSEL, France) with resolutions of 0.01 ℃, 0.01 pH unit, 0.10 μs cm^{-1}, and 0.01 mg L^{-1}, respectively. Concentration of HCO_3^- in each sample was titrated in the field using a portable alkalinity meter (Merck KGaACo., Germany) with a precision of 0.05 mmol L^{-1}.

The 500 mL high-density polyethylene (HDPE) bottles were used to store ion analyses samples filtering through

Table 1 Information of water samples

No	Types	Formations	Lithologies	Well depth (m)
W1	Groundwater wells	$Є_2m$	Pelitic dolostone, Limestone, Dolomite	77.85
W2	Groundwater wells	$Є_3z$-$Є_{2-3}m$	Limestone, Dolomite, Siltstone	196.40
W3	Groundwater wells	$Є_4O_1c$-$Є_3z$	Dolomitic limestone, Limestone	280.00
W4	Groundwater wells	$Є_3z$	Limestone	210.35
W5	Groundwater wells	$Є_3z$	Limestone	260.00
W6	Groundwater wells	$Є_3z$	Limestone	202.14
W7	Groundwater wells	$Є_4O_1c$-$Є_3z$	Dolomitic limestone, Limestone	251.00
W8	Groundwater wells	$Є_3z$	Limestone	230.00
W9	Groundwater wells	O_2w	Limestone, Dolomite	140.00
W10	Groundwater wells	O_2w	Limestone, Dolomite	200–233
W11	Groundwater wells	O_2d-$Є_4O_1s$	Marl, Dolomite	100.29
W12	Groundwater wells	O_2d-$Є_4O_1s$	Marl, Dolomite	203.03
W13	Groundwater wells	$Є_4O_1c$-$Є_3z$	Dolomitic limestone, Limestone	201.91
W14	Groundwater wells	$Є_4O_1c$	Dolomitic limestone, Limestone	110.00
S3	Spring	$Є_4O_1c$	Dolomitic limestone, Limestone	–
S1	Spring	$Є_3z$	Limestone	–
S2	Spring	$Є_3z$	Limestone	–

$Є_3z$, Cambrian Zhangxia Formation; $Є_{2-3}m$, Cambrian Mantou Formation; $Є_4O_1c$, Cambrian Chaomidian Formation; $Є_4O_1s$, Cambrian Sanshanzi Formation; O_2d, Ordovician Donghuangshan Formation; O_2w, Ordovician Wuyangshan Formation

0.45 μm-filter membranes. Water samples for cation measurements were acidified to pH < 2 using 1:1 HNO_3. The 50 mL HDPE brown bottles with screw caps were used to collect oxygen, hydrogen, nitrogen and carbon isotopic samples. All water samples were kept below 4 °C until they were analyzed.

All ions and other comprehensive parameters were analyzed by Seven multi pH/EC/ions integrated testing instrument, IRIS Intrepid II XSP ionomer spectrometer, visible spectrophotometer and iCAPQ ionomer mass spectrometer with a precision of 0.01 mg L^{-1} at the Key Laboratory of Karst Dynamics. Estimated analytical errors were within ±5%.

Hydrogen and oxygen isotopic values of water samples were measured by the high-precision laser spectroscopy (LWIA-24d, Los Gatos Research, USA) in the Key Laboratory of Karst Dynamics, all isotopic values were reported with respect to the Vienna Standard Mean Ocean Water (VSMOW). The measurement precisions for $\delta^{18}O$ and δD were 0.6‰ and 0.2‰, respectively.

Stable nitrogen and oxygen isotopes ($\delta^{15}N_{NO3}$ and $\delta^{18}O_{NO3}$) were measured using Gas-Bench- Mat 253 stable isotopes mass spectrometry (America, Therm corporation) with a precision of 0.3‰ in Third Institute of Oceanography, Ministry of Natural Resources. $\delta^{15}N_{NO3}$ and $\delta^{18}O_{NO3}$ were calibrated by the N_2 in atmosphere and VSMOW, respectively.

Stable carbon isotope of dissolved inorganic carbon ($\delta^{13}C_{DIC}$) was measured using MAT-253 mass spectrometer (America, Thermo Fisher company) with a precision of 0.15‰ in Third Institute of Oceanography, Ministry of Natural Resources. They were calibrated by the international standard Vienna Pee Dee Belemnite (VPDB).

Data preparation/treatment for discussion

It is a multivariate problem for the regional hydrogeochemical study because of the diverse variables associated. Multivariate statistical methods can provide inferred information of cause-and-effect relationships [20]. Descriptive statistical analyses of hydrogeochemical data and a set of graphical representations were used in the paper to explore hydrogeochemical characteristics, ion sources and associated major mechanisms influencing hydrogeochemical processes.

The unit of detected ion concentration is usually mg L^{-1} (milligram per litre), which should be converted into other units for analyzing the monitoring data. The value of ion in mmol L^{-1} (millimole per liter) could be calculated as ion concentration (mg L^{-1}) divided by relative atomic/molecular weight, it divided by charge number of the ion is the value of ion in meq L^{-1} (ρ, milli equivalent per litre). Each type of water samples was drawn separately in the analyzed graphs. Piper Diagram was plotted to analyze hydrochemistry types based on the percentages of major ions (meq L^{-1}, Ca^{2+}, Mg^{2+}, Na^+, K^+, CO_3^{2-}, HCO_3^-, Cl^- and SO_4^{2-}) with the help of Origin. Gibbs diagrams were mapped by the equivalence ratios of $\rho(Na^+)/\rho(Na^+ + Ca^{2+})$ and $\rho(Cl^-)/\rho(Cl^- + HCO_3^-)$ as a function of TDS, they were used to

analyze the natural sources of ions in groundwater system. Ions ratios of two or several hydrochemical components in different units, Cl^-/Na^+ versus NO_3^-/Na^+ (molar ratios), and Ca^{2+}/Na^+ versus HCO_3^-/Na^+ (molar ratios) were mapped with the help of statistic analyses platform to evaluate the hydrogeochemical evolution processes, the related separation lines referred to Lyu et al. [21] and Gomaah et al. [22]. The saturation index (SI) was computed with the geochemical program PHREEQC to evaluate the variation direction of water-rock interaction. Carbonate minerals could be dissolved by groundwater with the negative values of SI. Likewise, carbonate minerals could possibly precipitate with the positive values of SI [23]. Relationships between δD, ions, EC and $\delta^{18}O$ were plotted to interpret the influencing factors of groundwater chemical compositions. The deuterium excess parameter was proposed and defined as $d = \delta D - 8.00\ \delta^{18}O$ by Dansgaard [24], which was calculated to verify the recharging sources of groundwater in the basin. In order to trace the sources of NO_3^- in the groundwater system, $\delta^{15}N_{NO3}$ and $\delta^{18}O_{NO3}$ of water samples were mapped in typical ranges of isotopes values from various sources. DIC and its $\delta^{13}C_{DIC}$ were mapped in different carbonates dissolution processes to assess the origin of DIC in the carbonate system.

Results and discussion

Characteristics of water chemical compositions

TDS values of all water samples were lower than 500 mg L^{-1}. HCO_3^- is the main inorganic carbon species at pH between 6.98 and 7.80 [25]. CO_3^{2-} was not detected in any water sample, and groundwater in the study area is undersaturated with the respect to calcite and dolomite. The drinking-water standard of WHO for NO_3^- is not more than 50 mg L^{-1} falling between the standard values of drinking water (NO_3^-, 44.28 mg L^{-1}) and groundwater (NO_3^-, 88.56 mg L^{-1}) established by the People's Republic of China (PRC), and the taste impairment minimal level for SO_4^{2-} in both WHO and PRC is below 250 mg L^{-1} [26–28]. Concentrations of NO_3^- in six groundwater wells exceeded the guideline value (WHO), they were mainly located in the mid-down areas where have higher intensity of agriculture activities and larger amount of groundwater resources (Fig. 1a). Values of SO_4^{2-} in all water samples were much lower than the taste impairment minimal value.

Table 2 is the evaluation results of hydrochemistry types in water samples flowing through different formations. It can be noticed that the dominant hydrochemistry type in the study area was HCO_3–SO_4–Ca, while HCO_3–Ca was the dominant type in water samples formed in $Є_3z$ (Table 2). The Piper Diagram was plotted to illustrate the relative contents of major ions in water samples graphically (Fig. 3), it could be used to evaluate hydrogeochemical evolution processes [29]. All water samples fell in the area 5 (Fig. 3), both Ca^{2+}+ Mg^{2+} and HCO_3^-+ CO_3^{2-} contents exceeded the half of total cations and anions, respectively. HCO_3^- was the dominant anion because that all water samples were plotted in

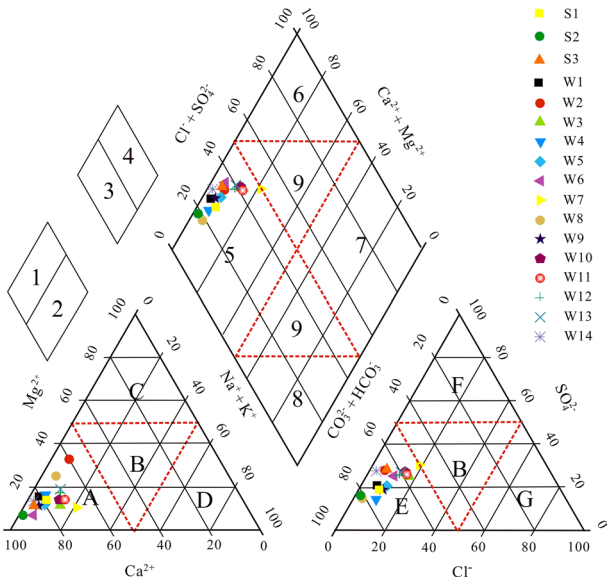

Fig. 3 The piper diagram of water samples

Table 2 The statistical table of hydrochemistry types in different stratums

No	Formations	Hydrochemistry types	No	Formations	Hydrochemistry types
S1	$Є_3z$	HCO_3–Ca	W7	$Є_4O_1c$– $Є_3z$	HCO_3–SO_4–Ca
S2	$Є_3z$	HCO_3–Ca	W13	$Є_4O_1c$–$Є_3z$	HCO_3–SO_4–Ca
S3	$Є_4O_1c$	HCO_3–SO_4–Ca	W3	$Є_4O_1c$	HCO_3–SO_4–Ca
W1	$Є_3z$-$Є_{2-3}m$	HCO_3–Ca	W14	$Є_4O_1c$	HCO_3–SO_4–Ca
W2	$Є_3z$-$Є_{2-3}m$	HCO_3–SO_4–Ca	W11	O_2d–$Є_4O_1s$	HCO_3–SO_4–Ca
W4	$Є_3z$	HCO_3–Ca	W12	O_2d–$Є_4O_1s$	HCO_3–SO_4–Ca
W5	$Є_3z$	HCO_3–Ca	W9	O_2W	HCO_3–Ca
W6	$Є_3z$	HCO_3–SO_4–Ca	W10	O_2W	HCO_3–SO_4–Ca
W8	$Є_3z$	HCO_3–Ca			

zone E (HCO_3^- type), it accounted for 51–81%, the second was SO_4^{2-} with the content of 14–30%, Cl^- was the least (2–19%). With respect to cations, all water samples fell in the zone A (Ca^{2+}), Ca^{2+} was the dominant cation accounting for 60–91%, Mg^{2+} was the second (7–32%), the least was $Na^+ + K^+$ (1–21%).

The dominant mechanisms proposed by Gibbs diagrams include precipitation, rock weathering and evaporation-crystallization processes [21]. Ionic concentrations in the analyzed part were standardized to be in milli equivalent per litre (ρ, meq L^{-1}). The equivalence ratios of $\rho(Na^+)/\rho(Na^+ + Ca^{2+})$ and $\rho(Cl^-)/\rho(Cl^- + HCO_3^-)$ as the function of TDS were plotted in Fig. 4. All water samples had medium TDS, low $\rho(Na^+)/\rho(Na^+ + Ca^{2+})$ and $\rho(Cl^-)/\rho(Cl^- + HCO_3^-)$, they fell in the middle left of Gibbs diagrams indicating that rock weathering dominated the chemical compositions of groundwater in the study area. The rock weathering type would be discussed furtherly in the following.

Major mechanisms of hydrogeochemical processes

Ions ratios analyses

Karst groundwater is the main water supply source for the local people in the study area. Understanding the hydrogeochemical processes is vital to use karst groundwater resources reasonably. Chemical compounds in groundwater and their relationships can interpret the origin chemical compositions and hydro-geochemical evolution processes [25, 29, 30]. Ions ratios of two components or several components were plotted in Fig. 5.

In the carbonate aquifers, Na^+ and K^+ have much lower concentrations than Ca^{2+} and Mg^{2+} in the foregoing discussion, they would probably come from dissolution of feldspars [25]. Values of $Na^+ + K^+/Cl^-$ in all water samples fell around the 1:1 line (Fig. 5a), verifying that major sources of Na^+ and K^+ were the dissolution of halite and sylvite furtherly [31].

There is a small amount of chloride and sulfate minerals in the strata of the basin. The values of total cations/$Cl^- + SO_4^{2-}$ would be close to 1 under the intensive human activities, because chloride salts (e.g. NaCl, $CaCl_2$) and sulfate salt (e.g. $MgSO_4$, $CaSO_4$) generated in the daily life, agricultural activity and industrial activity became man-made sources of Cl^- and SO_4^{2-} in the material circulation of groundwater system [29, 32]. However, all water samples lie above the 1:1 line in Fig. 5b indicating that human activities had little influence on Cl^- and SO_4^{2-} in the groundwater system. Only the dissolution of carbonate and silicate increase alkalinity and total major cations with nearly a 1:1 ratio in aquatic systems [32]. Because dissolution of salts (e.g. NaCl, $CaCl_2$) would not affect alkalinity [33], so the total major cations in Fig. 5c subtracted the equal Cl^- (meq L^{-1}). Carbonates (limestone and dolomite) are the dominant minerals of the aquifers in the study area (Table 1). The karst groundwater still has the ability of dissolving carbonate materials for the undetected CO_3^{2-} in the groundwater system. All water samples lie above the 1:1 line in Fig. 5c indicating that gypsum dissolution existed in the study area, resulting in the increased Ca^{2+} without an increase in alkalinity.

The major solute compositions in groundwater were dominated by Ca^{2+}, Mg^{2+}, HCO_3^- and SO_4^{2-}. The relationship lines of 1:1 and 1:2 in Fig. 5d describe the weathering of calcite and dolomite, respectively. All water samples fell inside the area between lines of 1:1 and 1:2 (Fig. 5d)

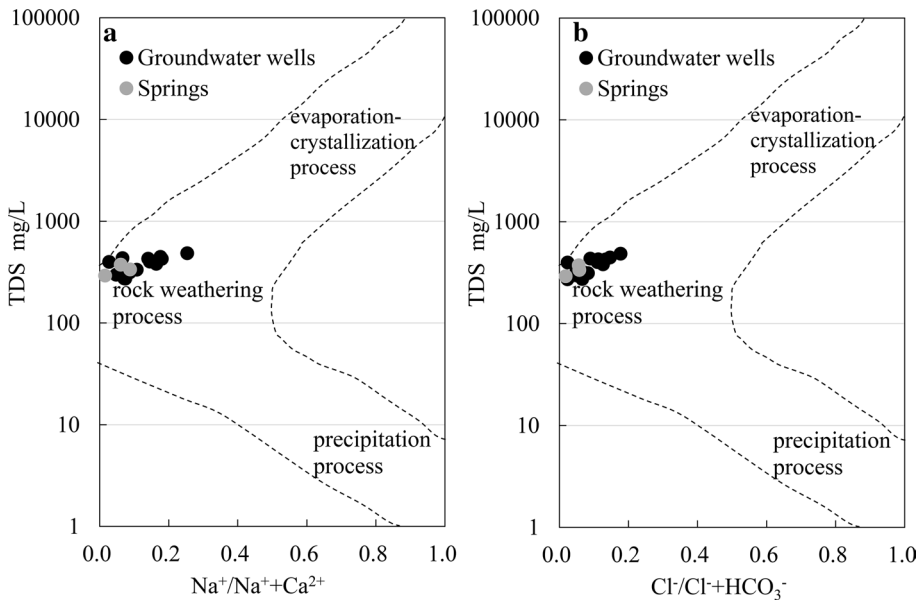

Fig. 4 Diagrammatic representation of processes controlling the chemistry of water samples in the area: **a** TDS versus $\rho(Na^+)/\rho(Na^+ + Ca^{2+})$, **b** TDS versus $\rho(Cl^-)/\rho(Cl^- + HCO_3^-)$

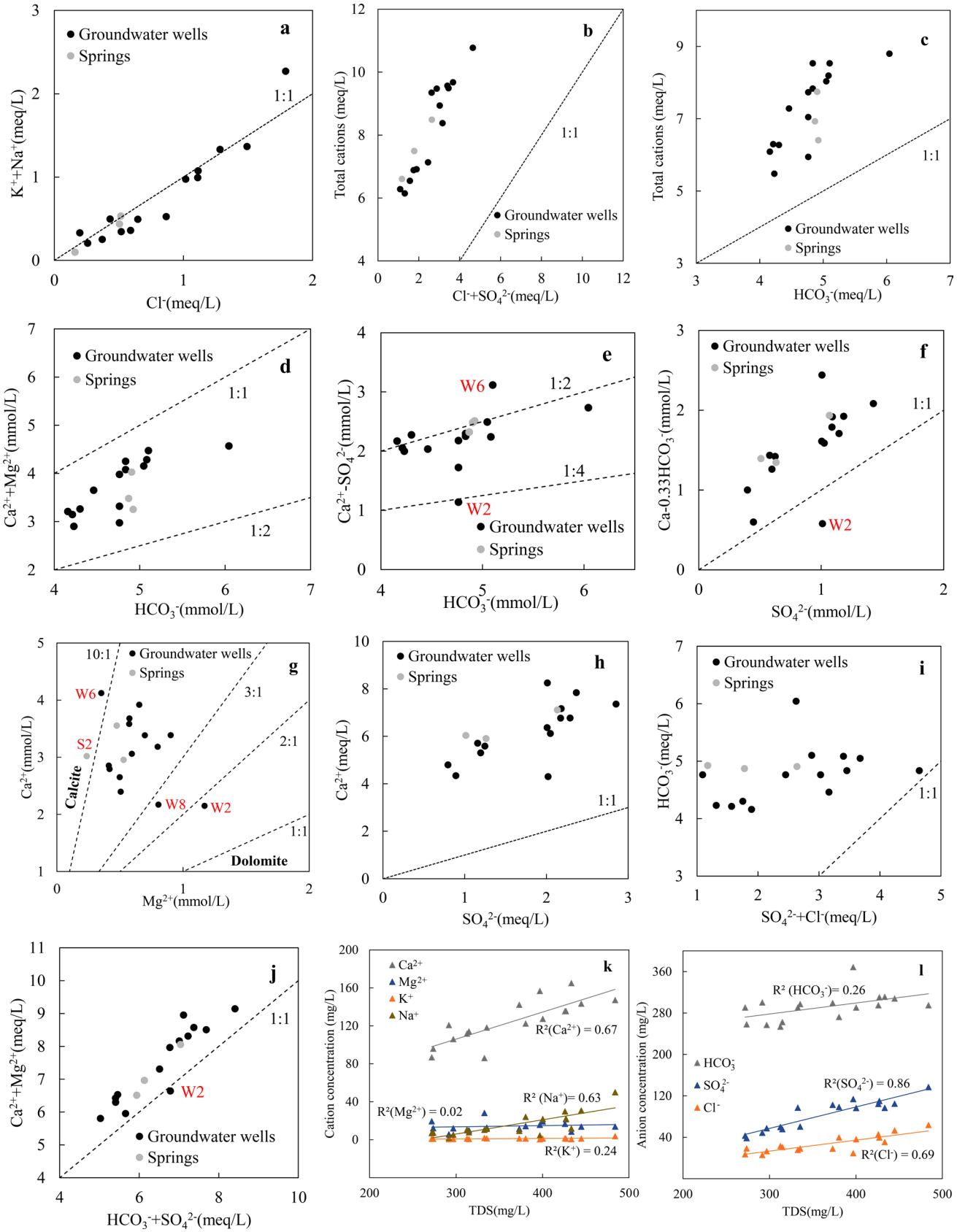
a
Groundwater wells
Springs
1:1
K+Na (meq/L)
Cl-(meq/L)
b
Total cations (meq/L)
1:1
Groundwater wells
Springs
Cl-+SO4 2-(meq/L)
c
Total cations (meq/L)
1:1
Groundwater wells
Springs
HCO3-(meq/L)
d
Groundwater wells
Springs
1:1
1:2
Ca2++Mg2+(mmol/L)
HCO3-(mmol/L)
e
W6
1:2
1:4
W2
Groundwater wells
Springs
Ca2+-SO4 2-(mmol/L)
HCO3-(mmol/L)
f
Groundwater wells
Springs
1:1
W2
Ca-0.33HCO3-(mmol/L)
SO4 2-(mmol/L)
g
10:1
Groundwater wells
Springs
W6
S2
3:1
2:1
Calcite
W8
W2
1:1
Dolomite
Ca2+(mmol/L)
Mg2+(mmol/L)
h
Groundwater wells
Springs
1:1
Ca2+(meq/L)
SO4 2-(meq/L)
i
Groundwater wells
Springs
1:1
HCO3-(meq/L)
SO4 2-+Cl-(meq/L)
j
1:1
W2
Groundwater wells
Springs
Ca2++Mg2+(meq/L)
HCO3-+SO4 2-(meq/L)
k
Ca2+
Mg2+
K+
Na+
R2(Ca2+) = 0.67
R2 (Na+)= 0.63
R2(Mg2+) = 0.02
R2(K+) = 0.24
Cation concentration (mg/L)
TDS(mg/L)
l
R2 (HCO3-)= 0.26
HCO3-
SO4 2-
Cl-
R2(SO4 2-) = 0.86
R2(Cl-) = 0.69
Anion concentration (mg/L)
TDS(mg/L)

◂**Fig. 5** Relationship between/among hydrochemical compositions: **a** Cl^- versus $K^+ + Na^+$. **b** $Cl^- + SO_4^{2-}$ versus total cations. **c** HCO_3^- versus total cations. **d** HCO_3^- versus $Ca^{2+} + Mg^{2+}$. **e** HCO_3^- versus $Ca^{2+} - SO_4^{2-}$. **f** SO_4^{2-} versus $Ca^{2+} - 0.33\ HCO_3^-$. **g** Mg^{2+} versus Ca^{2+}. **h** SO_4^{2-} versus Ca^{2+}. **i** $SO_4^{2-} + Cl^-$ versus HCO_3^-. **j** $HCO_3^- + SO_4^{2-}$ versus $Ca^{2+} + Mg^{2+}$. **k** TDS versus cation concentrations. **l** TDS versus anion concentrations

indicating that both calcite and dolomite weathering existed in the carbonate aquifers.

To evaluate the influences of dissolution of calcite, dolomite and gypsum on karst groundwater chemistries, non-gypsum source calcium was expressed as $Ca^{2+} - SO_4^{2-}$, non-carbonate source calcium was expressed as $Ca^{2+} - 0.33HCO_3^-$ [34]. The lines of 1:4 and 1:2 in Fig. 5e suggest the congruent dissolution of calcite and dolomite, respectively. Most of water samples were located between lines of 1:4 and 1:2, while they were closer to the 1:2 line (Fig. 5e), indicating that calcite dissolution had higher contribution to Ca^{2+} and HCO_{32}^- in groundwater. Water samples falling above the line 1:2 (Fig. 5e) had other sources of Ca^{2+} (e.g. $CaCl_2$, $CaSO_4$) generated by human activities besides calcite, dolomite and gypsum [29, 32]. The 1:1 line in Fig. 5f suggest the congruent dissolution of gypsum, all samples except W2 fell above the 1:1 line (Fig. 5f), indicating these water samples also have other sources of Ca^{2+} in the groundwater system. W6 is located at middle-downstream areas where have relatively higher human activities, it had much more sources of Ca^{2+} and deflected from the 1:2 line markedly (Fig. 5e). W2 is located at the border of Ar and $Є_{2+3}$ (Fig. 1a), groundwater in the well is the mixture dissolution of carbonates and other minerals (Table 1), and it deflected from the 1:4 line in Fig. 5e and the 1:1 line in Fig. 5f.

Mg^{2+} is mostly contributed by the weathering of dolomite in carbonate aquifers, Ca^{2+}/Mg^{2+} ratios can be used to analyze the relative proportions of calcite and/or dolomite dissolution [35]. Lines of 10:1, 3:1, and 1:1 in Fig. 5g describe dissolution of calcite, calcite and dolomite, and dolomite, respectively. Mostly water samples fell inside the lines of 10:1 and 1:1 and were closer to the 10:1 (Fig. 5g), ratios of Ca^{2+}/SO_4^{2-} and $HCO_3^-/SO_4^{2-} + Cl^-$ were greater than 1 (Fig. 5h, i), these information suggested that dolomite and gypsum dissolution would not be the primary sources of Ca^{2+} for water samples and chloride salts dissolution were weak. Thus, calcite dissolution dominated the water chemistries in the carbonate aquifers. Groundwater in W2 comes from dissolution of carbonates and other salts, and it was closer to the line of 1:1 in Fig. 5g.

If the dissolution of calcite, dolomite and gypsum are the major geochemical processes, ratios of $Ca^{2+} + Mg^{2+}/HCO_3^- + SO_4^{2-}$ would be close to 1:1. Most samples fell above and were closer to the 1:1 line in Fig. 5j, suggesting that major cations ($Ca^{2+} + Mg^{2+}$) had other sources in the carbonate systems besides the dissolution of calcite, dolomite and gypsum.

Relationships between TDS and major ions contents were shown in Fig. 5k, l. Ca^{2+} and HCO_3^- made the greatest contribution to TDS, followed by SO_4^{2-}, Cl^-, Na^+, Mg^{2+} and K^+. TDS had obvious positive correlations with Ca^{2+}, Na^+, SO_4^{2-} and Cl^-, it can be suggested that sources of Ca^{2+}, Na^+, SO_4^{2-} and Cl^- in the karst groundwater system were relatively stable.

Analyses of the Na^+ normalized Cl^- versus NO_3^- plot

Concentration ranges of NO_3^- in groundwater wells and springs were 14.91–87.31 mg L^{-1} and 28.48–48.26 mg L^{-1}, the average values were 44.52 mg L^{-1} and 40.11 mg L^{-1}, respectively. Springs water can be obtained in several meters under the earth's surface, the depth of groundwater wells ranges from 77 to 280 m (Table 1), so springs are much more vulnerable to NO_3^- contamination than groundwater wells. Nitrate is considered to be the particular pollutant of groundwater in agricultural areas [36], Cl^- is a conservative ion and also can be used to indicate the intensity of human activities [37], the Na^+ normalized Cl^- versus NO_3^- plot was mapped in Fig. 6 to interpret the influence factors of water samples in the basin.

All springs influenced by human activities was suggested by Fig. 6. Several groundwater wells (W1, W4, W5, W6, W9, W12 and W14) also fell in the human activities area (Fig. 6), they are distributed in both sides of Xinxue River from upstream to downstream (Fig. 1a), NO_3^- concentrations in some wells (W1, W5, W12, W9) were close to or higher than the WHO standard (50 mg L^{-1}). Even though the average value of NO_3^- concentrations in groundwater wells and springs did not exceed the 50 mg L^{-1}, it could be concluded from the foregoing analyses results that the carbonate aquifers in the basin were influenced by human activities regionally.

Analyses of the Na^+ normalized Ca^{2+} versus HCO_3^- plot

According to the foregoing analyses results, Ca^{2+} and HCO_3^- are the main cation and anion in the karst groundwater system, respectively. The Na^+ normalized Ca^{2+} vs. HCO_3^- diagram (Fig. 7) could be used to trace the rocks/minerals sources of Ca^{2+} and HCO_3^- in the basin [29]. It can be seen from Fig. 7 that all water samples fell in the areas between carbonate and silicate weathering. These processes were emphasized by relationships among $K^+ + Na^+$ and Cl^- (Fig. 5a), TDS and major ions (Fig. 5k, l). The analyzed result was in consistent with ions ratios analyses results.

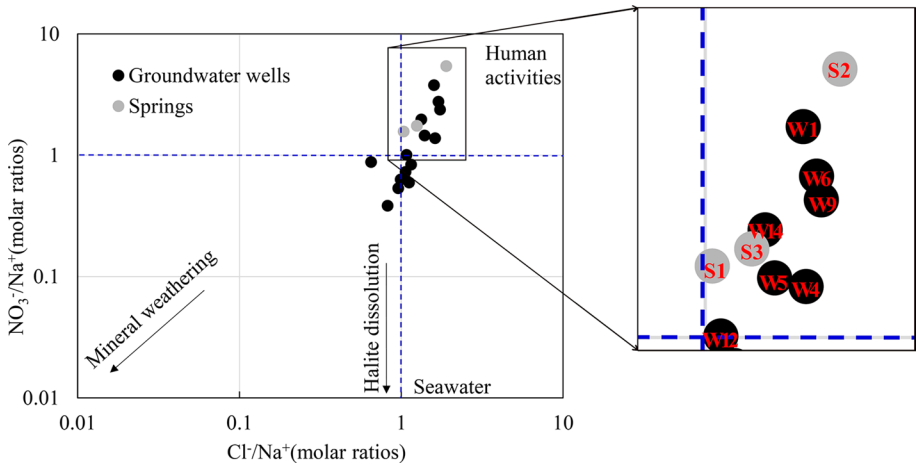

Fig. 6 Plot of the Cl^-/Na^+ molar ratios versus NO_3^-/Na^+ molar ratios for groundwater wells and springs

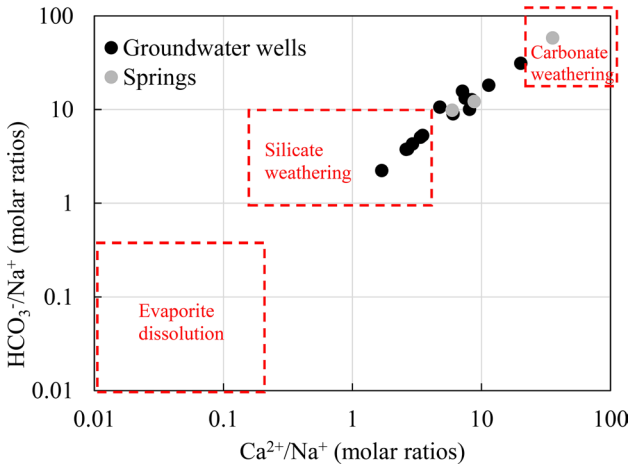

Fig. 7 Plot of the Ca^{2+}/Na^+ molar ratios versus HCO_3^-/Na^+ molar ratios for groundwater wells and springs

Analyses of δD and $\delta^{18}O$ in karst groundwater and precipitation

Meteorological processes affected hydrogen and oxygen isotopes of hydrological system. Groundwater cycle information can be interpreted by characteristics of δD and $\delta^{18}O$. The global meteoric water line (GMWL) ($\delta D = 8\delta^{18}O + 10$) was proposed by Craig [38]. The deuterium excess parameter was calculated by using the equation of $d = \delta D - 8\delta^{18}O$ [24].

Relationships of δD and $\delta^{18}O$ in karst groundwater and precipitation

The local meteoric water lines (LMWL, $\delta D = 6.30\delta^{18}O - 3.63$) was obtained based on δD and $\delta^{18}O$ isotopic values of precipitation provided by global network of isotopes in precipitation (GNIP). LMWL, cross-plot of *d* values, δD and $\delta^{18}O$ of sampling points and their regression line were plotted in Fig. 8. All water samples fell near and below the LMWL (Fig. 8), the regression equation of them was $\delta D = 5.73\delta^{18}O - 12.23$, whose slope factor was close to the LMWL, suggesting that carbonate aquifers were the meteoric origin with weak evaporation [29, 39].

Water samples plotted in Fig. 8 could be divided into two groups. Group A consists of S2, S3, W1, W2, W6, W8 and W9 with δD values ranging from −61.90 to −57.80‰ and $\delta^{18}O$ values ranging from −8.59 to −8.30‰, average values

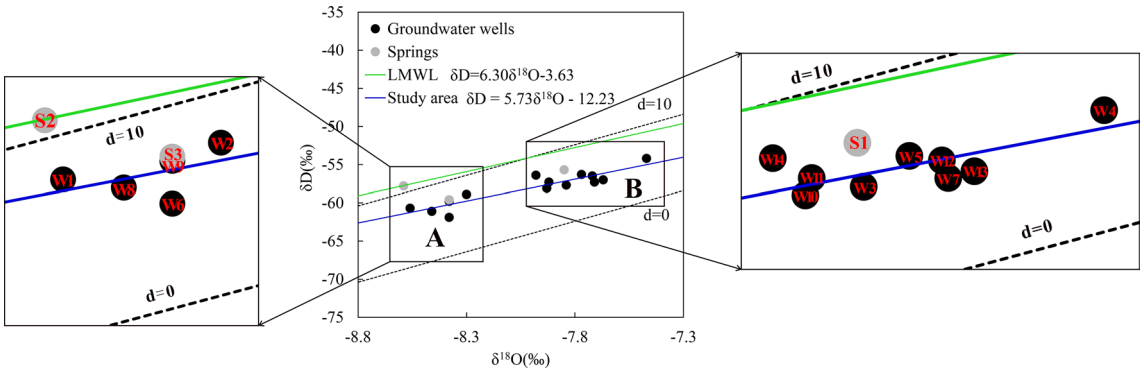

Fig. 8 LMWL, δD and $\delta^{18}O$ of sampling points and their regression line

of δD and $\delta^{18}O$ were − 59.97‰ and − 8.43‰, respectively. Group B consists of S1, W3, W4, W5, W7, W10, W11, W12, W13 and W14 with δD values ranging from − 58.10 to 54.20‰ and $\delta^{18}O$ values ranging from − 7.98 to − 7.47‰, average values of δD and $\delta^{18}O$ were − 56.65 and − 7.77‰, respectively. Values of δD and $\delta^{18}O$, average values of δD and $\delta^{18}O$ in group B were higher than those in group A, the reasons would be discussed in the following.

Interactions between water and rock occur once that precipitation enters the carbonate aquifer system. Light isotopes with lower atomic mass take part in hydrogeochemical processes preferentially, heavy isotopes would be in the residual part. Therefore, D and ^{18}O would become much richer along the flow path or through the intensive hydrodynamic regions.

Sampling points in group B (Fig. 8) had the closer relationship with surface water, precipitation, upper non-carbonate groundwater and other external factors, their hydrogeochemical processes were much more complex. The spatial distribution positions of the river are the main flow paths of karst groundwater in the basin, where S1, W3, W4, W5 and W7 in group B are mainly distributed along the Xinxue River, so they have much more frequently interactions with surface water and precipitation. The dropping process of rainwater and the flow process of Xinxue River experienced evaporation, processes of rainwater recharging groundwater and surface water interacting with groundwater also experienced complex hydrogeochemical reactions. W10, W11, W12, W13 and W14 in group B are located at the Yangzhuang block where has the largest quantity of karst groundwater in the basin (Fig. 1a) and the strongest hydrodynamic conditions, because that the block has more complex recharging ways of upper underground runoff, surface water and precipitation.

Other water sampling points in group A have a distance away from Xinxue River and are scattered in the basin, the positions where they are located have relatively low yield property of aquifer with weak karst development characteristics [19] (Fig. 1a). Groundwater in these samples were mainly affected by the evaporation of precipitation and water-rock interaction. Thus, it can be seen from Fig. 8 that sampling points in group A were much closer to the LMWL.

The *d* values in the carbonate aquifers

Groundwater is inherited from the precipitation if *d* values of groundwater fall inside the range of precipitation [40]. Table 3 showed that the range of *d* values of all water samples fell inside the range of precipitation in the basin, it emphasized that the precipitation was the origin of karst groundwater resources in the basin.

The *d* parameter is the function of the exchange degree of oxygen isotope between water and rock, groundwater residence time and hydrogeological condition [4]. The *d* value decreases with the longer time of water-rock interactions and the higher groundwater residence time, which was proved by the statistical table of *d* values in different types furtherly (Table 3). The flow path of precipitation recharging springs was shorter compared with groundwater wells, hydrodynamic conditions and hydrogeochemical processes in group A were simpler than group B. Thus, highest, lowest and mean values of springs and group A were higher than groundwater wells and group B, respectively (Table 3).

Table 3 The statistical table of *d* values in different types

Types	*d* values (‰)		
	Highest value	Lowest value	Mean value
Precipitation	22.00	3.80	9.39
All water samples	10.92	4.36	6.41
Groundwater wells	7.78	4.36	5.96
Springs	10.92	7.10	8.49
Group A	10.92	5.14	7.51
Group B	7.44	4.36	5.64

The *d* is also an indicator of kinetic fractionation during evaporation, it is more useful to interpret the evaporation in modifying the isotopic character of rainwater prior to groundwater [24, 40]. The $d = 10‰$ line in Fig. 8 coincides with the GMWL. The *d* values in almost all water samples were less than 10‰ (Fig. 8), the average value of water samples (6.41‰) was lower than the precipitation (9.39‰) (Table 3). It can be concluded that evaporation existed in the precipitation recharging groundwater, which was the same with isotopes analyses results.

Relationships between $\delta^{18}O$ and karst groundwater salinity

Stable isotopes have been used in detecting the origin and possible mechanisms of groundwater salinity successfully [41]. Groundwater salinity in the study area increases in function of the path distance or groundwater movement, concentrations of ions and hydrochemistry types would generally change, groundwater isotopic evolution depends on the ratio of admixed water members or evaporation rates [42].

The amount of hydrogen is small in rocks or formations, the oxygen would play a key role in the water-rock interaction process and have a certain relationship with groundwater salinity [4]. Relationships between Ca^{2+}, Mg^{2+}, Na^{+}, K^{+}, HCO_3^{-}, SO_4^{2-}, Cl^{-}, NO_3^{-}, EC and $\delta^{18}O$ were shown in Fig. 9, it can be seen from the figure that

two enrichment processes existed in the study area. The one was evaporation process, which affected W4 and had some extent influences on W5 and W8. The other one was the combination of evaporation and dissolution processes, which affected W1, W2, W3, W6, W7, W9, W10, W11, W12, W13, W14 and all springs principally. Areas where W4, W5 and W8 were located have lower yield property of aquifer and weaker groundwater flow intensity (Fig. 1a). Other water samples had higher average TDS (381.26 mg L^{-1}) than W4 (273.50 mg L^{-1}) or the average value of W5 and W8 (292.20 mg L^{-1}). It can be concluded that the isotopic values and groundwater salinity were mainly enriched by the combination of evaporation and dissolution processes, which was coincided with the foregoing analyses results.

Analyses of $\delta^{15}N_{NO3}$ and $\delta^{18}O_{NO3}$ in karst groundwater

Yangzhuang karst groundwater basin were influenced by human activities regionally based on the foregoing analyses results. Whereas NO_3^- was the most representative ion in the basin, relationships between $\delta^{15}N_{NO3}$ and $\delta^{18}O_{NO3}$ of sampling points were mapped in Fig. 10 to interpret the sources characteristics of NO_3^- in the basin. $\delta^{15}N_{NO3}$ ranged from −2.37 to 8.36‰ with the mean value of 1.18‰, $\delta^{18}O_{NO3}$

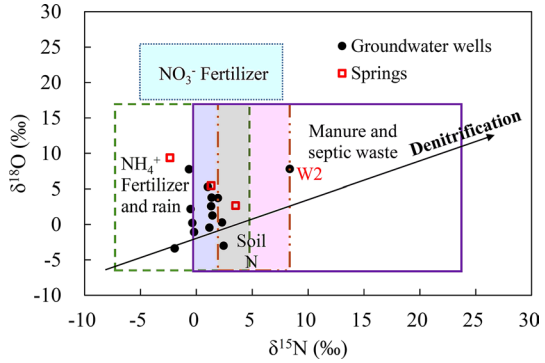

Fig. 10 $\delta^{15}N_{NO3}$ relative to $\delta^{18}O_{NO3}$ of monitoring points and typical ranges of isotopes values from various sources

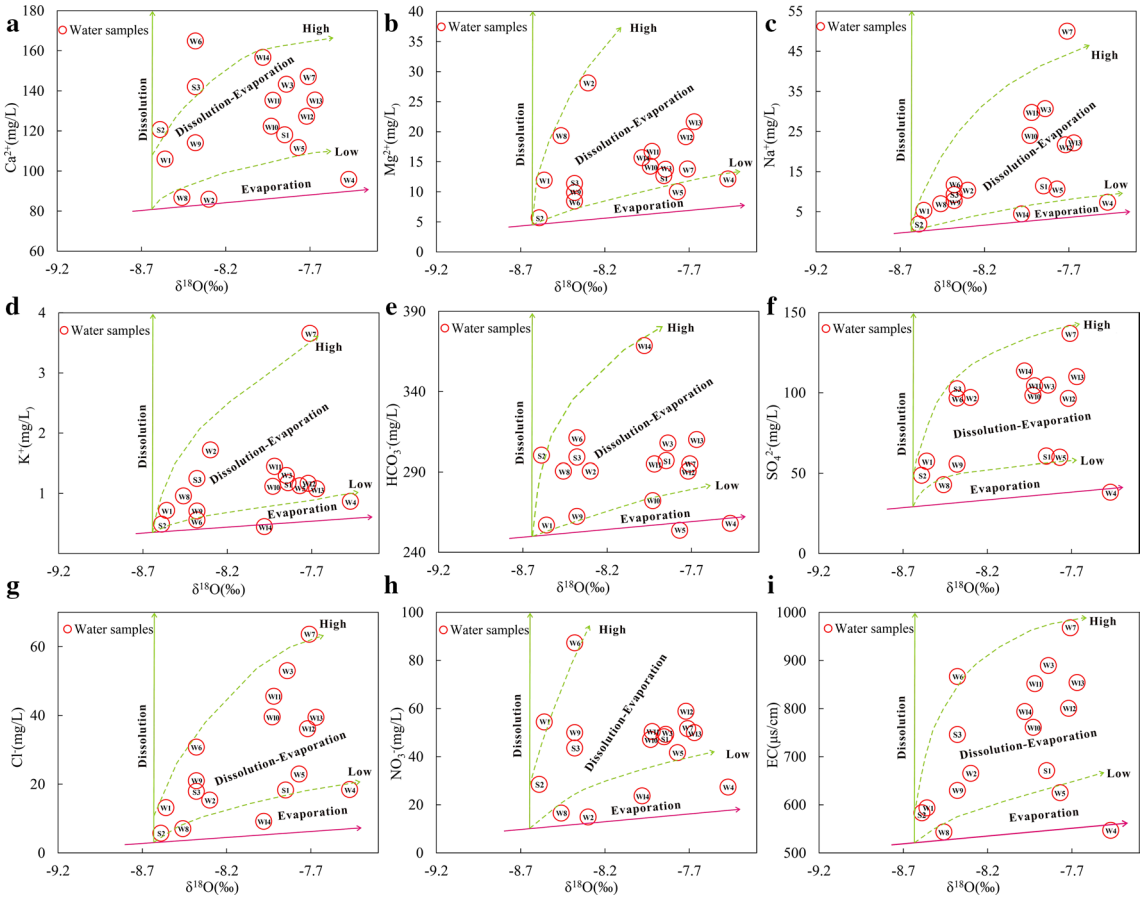

Fig. 9 Relationships between average concentrations of Ca^{2+} and $\delta^{18}O$ (**a**), Mg^{2+} and $\delta^{18}O$ (**b**), Na^+ and $\delta^{18}O$ (**c**), K^+ and $\delta^{18}O$ (**d**), HCO_3^- and $\delta^{18}O$ (**e**), SO_4^{2-} and $\delta^{18}O$ (**f**), Cl^- and $\delta^{18}O$ (**g**), NO_3^- and $\delta^{18}O$ (**h**), and EC values versus $\delta^{18}O$ (**i**). The green lines represent evolutions related to low and high salinity increase

ranged from − 3.39 to 9.37‰ with the mean value of 2.60‰.

All samples fell into the ranges of fertilizer and soil except W2 (Fig. 10). Generally, $\delta^{15}N_{NO3}$ was higher than 10‰ in the animal sources [43], while W2 is located in a chestnut factory with $\delta^{15}N_{NO3}$ value of 8.36‰. Thus, NO_3^- in W2 was mostly recharged by septic waste. Figure 10 illustrated that NO_3^- in groundwater mostly fell into the range of fertilizer. Agriculture is the main landuse type in the basin, N inorganic fertilizer was applied into the fields by the local inhabitants. The volatilization and nitrification of N inorganic fertilizer could make $\delta^{15}N_{NO3}$ and $\delta^{18}O_{NO3}$ within the range of soil-N [44]. It could be concluded that NO_3^- in groundwater of Yangzhuang karst groundwater basin mainly come from NH_4^+ fertilizer by human activities. The analyses results were same with the ions analyses of the Na^+ normalized Cl^- versus NO_3^- plot.

$\delta^{13}C_{DIC}$ characteristics of karst groundwater

DIC and $\delta^{13}C_{DIC}$ of groundwater are determined by hydrogeochemical processes in the carbonate aquifer system [45]. They could be used to assess the origin of DIC in the karst groundwater system. The carbonate aquifers in the basin could be treated as a closed system compared with the surface system [25]. DIC mostly came from the dissolution of carbonate minerals and soil CO_2 through the biodegradation of organic matters [45, 46], while the carbonate mineral precipitation is the main reason for removing DIC in the karst aquiferous system [45]. Moreover, $\delta^{13}C_{DIC}$ values are influenced by the fractionation, transformation or the mixture of different sources [45].

CO_3^{2-} and OH^- were not detected in the sampling points. The average value of pH was 7.08, H^+ with the concentration of $10^{-7.08}$ mol L^{-1} could be ignored in the calculation of alkalinity. Alkalinity was equal to the concentration of HCO_3^- in the basin. Relationship between alkalinity/DIC and $\delta^{13}C_{DIC}$ and the occurrent processes in the karst groundwater system were mapped in Fig. 11.

$\delta^{13}C$ values of carbonate minerals ranged from − 1.50 to − 7.80‰ [47, 48] with the average value of − 2.00‰ [25]. $\delta^{13}C_{DIC}$ would be 1.20‰ for the isotopic fractionation during the dissolution of carbonates [45], and line 1 was plotted in Fig. 11. Particulate organic carbon (POC) was ^{13}C-depleted with the $\delta^{13}C$ value of − 26.60‰ [48], open system equilibration of DIC with CO_2 would enrich $\delta^{13}C_{DIC}$ by about 9‰, and line 3 with the $\delta^{13}C_{DIC}$ value of − 17.60‰ was plotted in Fig. 11. Line 2 was the intermediate $\delta^{13}C_{DIC}$ with value of − 12.70‰ (Fig. 11).

$\delta^{13}C_{DIC}$ in the karst groundwater system varied from − 8.22 to − 14.15‰ with the mean value of − 11.96‰. $\delta^{13}C_{DIC}$ of sampling points were located between two end members and around the line 2, and they were mostly

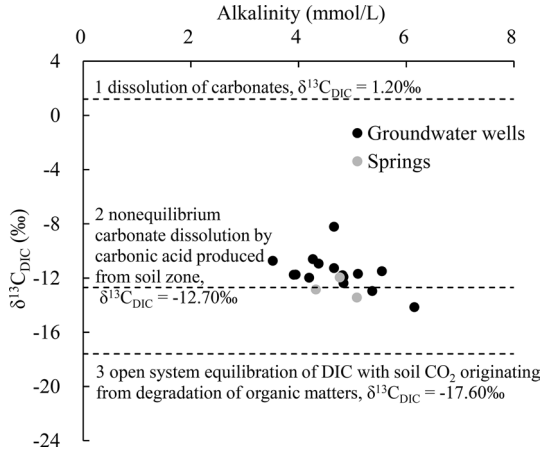

Fig. 11 Relationship between alkalinity and $\delta^{13}C_{DIC}$ of sampling points, the dotted lines were the occurrent processes in the karst groundwater system

located between line 1 and line 2 (above the − 12.70‰) (Fig. 11), suggesting carbonates dissolution had a greater contribution. Soil CO_2 had a greater contribution to sampling points located between line 2 and line 3 (below the − 12.70‰). The contribution range of carbonates dissolution was 44.78−66.12% with the average value of 52.92% based on the simple mass balance equations performed by Verbovšek and Kanduč [25].

Conclusions

Fracture-karst groundwater is the most important urban water supply in North China, hydrogeochemical characteristics in Yangzhuang karst groundwater basin can provide valuable suggestions for protecting and utilizing the local groundwater resources.

The dominant hydrochemistry type was HCO_3–SO_4-Ca in the carbonate aquifers of the basin. Dissolution of calcite, dolomite, gypsum and chloride salts existed in the carbonate aquifers. Ca^{2+} and HCO_3^- were the dominant cation and anion in the basin, respectively, they made the greatest contribution to TDS. Carbonates dissolution had relatively higher contribution to the sources of alkalinity (HCO_3^-), whereas calcite dissolution had higher contribution to Ca^{2+} and HCO_3^- in the karst groundwater system. Thus, carbonates dissolution (especially calcite dissolution) as the main rock chemical weathering dominated the chemical compositions of the karst groundwater system.

Values of δD and $\delta^{18}O$ in sampling points have the positive relationship with the influences of external factors, the intensity of hydrodynamic conditions, the complexity of hydrogeochemical processes and the time of water-rock

interactions. The atmospheric precipitation is the origin source of the karst groundwater system, its recharging processes had weak evaporation. Hydrogeochemical processes of the basin were mainly carbonates dissolution accompanied with weak evaporation during the recharging of atmospheric precipitation.

As the representative pollutant of groundwater in agricultural areas, NO_3^- in the karst groundwater of the basin mainly came from NH_4^+ fertilizer applied by local inhabitants. Although human activities had weak influence on the carbonate aquifers, they have affected the basin regionally at present. It is vital to take appropriate actions to prevent the deterioration of karst groundwater resources.

Acknowledgements Financial support was provided by the National Natural Science Foundation of China (41702277), Foundation of Guangxi Province (2017GXNSFFA198006, 2018GXNSFDA050002, 2018-242-Z01, AD17129047), Special Fund for Basic Scientific Research of Chinese Academy of Geological Sciences (JYYWF20182002, 2020004), UNESCO/IUGS (IGCP 661), Global Karst Resource Ecology United laboratory-Comparative study of classical karst areas between China and Slovenia (KY201802009), The national key research and development program of China (2016YFC0502306), the Geological Survey Projects of CGS (DD20190022, DD20190452). Authors thanks Dewang Jia, Jinliang Wang, Yongliang Liu, Bintao Liu, Laimou Lu and Yawei Feng for their assistance in field work. The authors would like to thank the editor and two anonymous reviewers for their constructive comments, which helped us improve the quality of the paper.

References

1. Marić N, Matić I, Papić P, Beškoski VP, Ilić M, Gojgić-Cvijović G, Miletić S, Nikić Z, Vrvić MM (2018) Natural attenuation of petroleum hydrocarbons—a study of biodegradation effects in groundwater (Vitanovac, Serbia). Environ Monit Assess 190:89
2. Iván V, Mádl-Szőnyi J (2017) State of the art of karst vulnerability assessment: overview, evaluation and outlook. Environ Earth Sci 76:112
3. Liang YP, Gao XB, Zhao CH, Tang CL, Shen HY, Wang ZH, Wang YX (2018) Review: characterization, evolution, and environmental issues of karst water systems in Northern China. Hydrogeol J 26:1371–1385
4. Guo YL, Wu Q, Jiang GH, Han ZW, Tang QJ, Quan XQ (2019) Dynamic variation characteristics of water chemistries and isotopes in a typical karst aquiferous system and their implications for the local karst water cycle, Southwest China. Carbonate Evaporite 34(3):987–1001
5. Sun ZY, Ma Y, Wang YX, Ma T, Liu YD (2016) Using isotopic, hydrogeochemical-tracer and temperature data to characterize recharge and flow paths in a complex karst groundwater flow system in northern China. Hydrogeol J 24:1393–1412
6. Pavlovskiy I, Selle B (2015) Integrating hydrogeochemical, hydrogeological, and environmental tracer data to understand groundwater flow for a karstified aquifer system. Groundwater 53:156–165
7. Huang H, Chen ZH, Wang T, Xiang CJ, Zhang L, Zhou GM, Sun BT, Wang Y (2019) Nitrate distribution and dynamics as indicators to characterize karst groundwater flow in a mined mineral deposit in southwestern China. Hydrogeol J 27:2077–2089
8. Jebreen H, Wohnlich S, Banning A, Wisotzky F, Niedermayr A, Ghanem M (2018) Recharge, geochemical processes and water quality in karst aquifers: Central West Bank, Palestine. Environ Earth Sci 77:261
9. Wang W, Zhang GH, Liu CH (2018) Using environmental isotopes to evaluate the renewable capacity of a typical karst groundwater system in northern China. Environ Earth Sci 77:257
10. Qian JZ, Peng YX, Zhao WD, Ma L, He XR, Lu YH (2018) Hydrochemical processes and evolution of karst groundwater in the northeastern Huaibei Plain, China. Hydrogeol J 26:1721–1729
11. Luo MM, Chen ZH, Zhou H, Zhang L, Han ZF (2018) Hydrological response and thermal effect of karst springs linked to aquifer geometry and recharge processes. Hydrogeol J 26:629–639
12. Vasić L, ·Živojinović D·Rajaković–Ognjanović V (2020) Hydrochemical changes and groundwater grouping data by multivariate statistical methods within one karst system: recharge–discharge zone (Eastern Serbia case study). Carbonate Evaporite 35:15
13. Rman N (2016) Hydrogeochemical and isotopic tracers for identification of seasonal and long-term over-exploitation of the Pleistocene thermal waters. Environ Monit Assess 188:242
14. Jiang YJ, Cao M, Yuan DX, Zhang YZ, He QF (2018) Hydrogeological characterization and environmental effects of the deteriorating urban karst groundwater in a karst trough valley: Nanshan, SW China. Hydrogeol J 26:1487–1497
15. Han XR (2015) Karst hydrogeology. Science Press, Beijing
16. Bu H, Chen ZC, Zhang LP (2008) Division of the drinking water source protection areas: take Shandong Yangzhuang groundwater basin as an example. Geol Surv Res 31(3):236–241
17. Fu XG, Tang ZH, Lv WB, Wang XM, Yan BZ (2018) Exploitation Potential of groundwater in Yangzhuang Basin, China Under Recharge Enhancement. Int J Heat Technol 36(2):483–493
18. Feng YW, Li ZF (2018) Evaluation of groundwater environmental evolution trend in the karst water system of Yangzhuang, Shandong Province. J Geol 42(4):662–667
19. Guo YL, Zhai YZ, Wu Q, Teng YG, Jiang GH, Wang JS, Guo F, Tang QJ, Liu SH (2016) Proposed APLIE method for groundwater vulnerability assessment in karst-phreatic aquifer, Shandong Province, China: a case study. Environ Earth Sci 75(2):112
20. Monjerezi M, Vogt RD, Aagaard P, Saka JDK (2011) Hydrogeochemical processes in an area with saline groundwater in lower Shire River valley, Malawi: an integrated application of hierarchical cluster and principal component analyses. Appl Geochem 26(8):1399–1413
21. Lyu M, Pang ZH, Huang TM, Yin LH (2019) Hydrogeochemical evolution and groundwater quality assessment in the Dake Lake Basin, Northwest China. J Radioanal Nucl Ch 320:865–883
22. Gomaah M, Meixner T, Korany EA, Garamoon H, Gomaa MA (2016) Identifying the sources and geochemical evolution of groundwater using stable isotopes and hydrogeochemistry in the Quaternary aquifer in the area between Ismailia and El Kassara canals, Northeastern Egypt. Arab J Geosci 9:437
23. Lin Y, Ren HX, Wu YZ, Cao FL, Jia FJ, Qu PC (2019) The evolution of hydrogeochemical characteristics of a typical piedmont karst groundwater system in a coal–mining area, Northern China. Environ Earth Sci 78:557
24. Dansgaard W (1964) Stable isotopes in precipitation. Tellus 16:436–468
25. Verbovšek T, Kanduč T (2016) Isotope geochemistry of groundwater from fractured dolomite aquifers in Central Slovenia. Aquat Geochem 22:131–151
26. WHO (World Health Organization) (2017) Guidelines for drinking-water quality: fourth edition incorporating the first addendum. CC BY-NC-SA, Licence 3.0 IGO

27. GB 5749-2006 (2006) Quality standard for drinking water. Ministry of Environmental Protection of the People's Republic of China
28. DZ/T 0290-2015 (2015) Standard for groundwater quality. Ministry of Natural Resources of the People's Republic of China
29. Huang XJ, Wang GC, Liang XY, Cui LF, Ma L, Xu QY (2018) Hydrochemical and stable isotope (δD and $\delta^{18}O$) characteristics of groundwater and hydrogeochemical processes in the Ningtiaota Coalfeld, Northwest China. Mine Water Environ 37:119–136
30. Yoshimoto S, Ishida S, Kobayashi T, Koda K, Tsuchihara T, Shirahata K (2020) Using hydrogeochemical indicators to interpret groundwater flow and geochemical evolution of a freshwater lens on Majuro Atoll, Republic of the Marshall Islands. Hydrogeol J. https://doi.org/10.1007/s10040-019-02105-w
31. Shen ZL, Zhu WH, Zhong ZS (1986) Fundamental hydrogeochemistry. Geological Publishing House, Beijing
32. Kim K, Rajmohan N, Kim HJ, Kim SH, Hwang GS, Yun ST, Gu B, Cho MJ, Lee SH (2005) Evaluation of geochemical processes affecting groundwater chemistry based on mass balance approach: a case study in Namwon, Korea. Geochem J 39(4):357–369
33. Garrels RM, Mackenzie FT (1967) Origin of the chemical compositions of some springs and lakes. Adv Chem 67(10):222–242
34. Wang YX, Guo QH, Su CL, Ma T (2006) Strontium isotope characterization and major ion geochemistry of karst water flow, Shentou, northern China. J Hydrol 328:592–603
35. Zavadlav S, Kanduč T, McIntosh J, Lojen S (2013) Isotopic and chemical constraints on the biogeochemistry of dissolved Inorganic carbon and chemical weathering in the Karst Watershed of Krka River (Slovenia). Aquat Geochem 19:209–230
36. Henson WR, Huang L, Graham WD, Ogram A (2017) Nitrate reduction mechanisms and rates in an unconfined eogenetic karst aquifer in two sites with different redox potential. Journal of Geophysical Research: Biogeosciences 122:1062–1077
37. Squillace PJ, Moran MJ (2007) Factors associated with sources, transport, and fate of volatile organic compounds and their mixtures in aquifers of the United States. Environ Sci Technol 41(7):2123–2130
38. Craig H (1961) Isotopic variations in meteoric waters. Science 133(3465):1702–1703
39. Asmael NM, Huneau F, Garel E, Celle-Jeanton H, Le Coustumer P, Dupuy A, Hamid S (2015) Origin and recharge mechanisms of groundwater in the upper part of the Awaj River (Syria) based on hydrochemistry and environmental isotope techniques. Arab J Geosci 8(12):10521–10542
40. Deshpande R, Bhattacharya S, Jani R, Gupta SA (2003) Distribution of oxygen and hydrogen isotopes in shallow groundwaters from Southern India: influence of a dual monsoon system. J Hydrol 271:226–239
41. Carrasco-Cantos F (2015) Application of stable isotopes ($\delta^{34}S$–SO_4, $\delta^{18}O$–SO_4, $\delta^{15}N$–NO_3, $\delta^{18}O$–NO_3) to determine natural background and contamination sources in the Guadalhorce River Basin (southern Spain). Sci Total Environ 506:46–57
42. Kattan Z (2018) Using hydrochemistry and environmental isotopes in the assessment of groundwater quality in the Euphrates alluvial aquifer, Syria. Environ Earth Sci 77:45
43. Spaldinga RF, Hirshb AJ, Exnerc ME, Littled NA, Kloppenborge KL (2019) Applicability of the dual isotopes $\delta^{15}N$ and $\delta^{18}O$ to identify nitrate in groundwater beneath irrigated cropland. J Contam Hydrol 220:128–135
44. Margalef-Marti R, Carrey R, Viladés M, Jubany I, Vilanova E, Graue R, Soler A, Oteroa N (2019) Use of nitrogen and oxygen isotopes of dissolved nitrate to trace fieldscale induced denitrification efficiency throughout an in-situ groundwater remediation strategy. Sci Total Environ 686:709–718
45. Kanduč T, Grassa F, McIntosh J, Stibilj V, Ulrich-Supovec M, Supovec I, Jamnikar S (2014) A geochemical and stable isotope investigation of groundwater/surface-water interactions in the Velenje Basin, Slovenia. Hydrogeol J 22:971–984
46. Kanduč T, Ogrinc N (2007) Hydrogeochemical characteristics of the River Sava watershed in Slovenia. Geologija 50(1):157–177
47. Garlick GD, Epstein S (1966) The isotopic composition of oxygen and carbon in hydrothermal minerals at Butte, Montana. Econ Geol 61:1325–1335
48. Parker SR, Gammons CH, Smith MG, Poulson SR (2012) Behavior of stable isotopes of dissolved oxygen, dissolved inorganic carbon and nitrate in groundwater at a former wood treatment facility containing hydrocarbon contamination. Appl Geochem 27:1101–1110